PTEP

Prog. Theor. Exp. Phys. **2013**, 00000 (26 pages)
DOI: 10.1093/ptep/0000000000

A model of charmed baryon-nucleon potential and 2- and 3-body bound states with charmed baryon

Saori Maeda[1,*], Makoto Oka[1,2], Akira Yokota[1], Emiko Hiyama[3], and Yan-Rui Liu[4]

[1]*Department of Physics, Tokyo Institute of Technology, O-okayama 2-12-1, Meguro, Tokyo 152-8551, Japan*
[2]*Advanced Science Research Center, Japan Atomic Energy Agency, Tokai, Ibaraki 319-1195, Japan*
[3]*Nishina Center for Accelerator-Based Science, The institute of Physical and Chemical Research(RIKEN), Wako 351-0198, Japan*
[4]*Department of Physics, Shandong University, Jinan, Shandong 250100, China*
[*]*E-mail: s-maeda@th.phys.titech.ac.jp*

A potential model for the interaction between a charmed baryon (Λ_c, Σ_c, and Σ_c^*) and the nucleon (N) is constructed. The model contains a long-range meson (π and σ) exchange part and a short-distance quark exchange part. The quark cluster model is used to evaluate the short-range repulsion and a monopole type form factor is introduced to the long-range potential to reflect the extended structure of hadrons. We determine the cutoff parameters in the form factors by fitting the NN scattering data with the same approach and we obtain four sets of parameters (a – d). The most attractive potential (d) leads to bound $\Lambda_c N$ states with $J^\pi = 0^+$ and 1^+ once the channel couplings among Λ_c, Σ_c and Σ_c^* are taken into account. One can also investigate many-body problems with the model. Here, we construct an effective $\Lambda_c N$ one-channel potential with the parameter set (d) and apply it to the 3-body $\Lambda_c NN$ system. The bound states with $J = 1/2$ and $3/2$ are predicted.

1. Introduction

Recent development of hadron spectroscopy revealed that there may exist various molecular bound states of hadrons (observed as hadron resonances) . In particular, the observation of the unexpected X, Y, and Z mesons and the follow by theoretical studies indicates that heavy quark molecules are more plausible. This can be understood from the balance between the kinetic term and the potential in the Hamiltonian: a heavier system has a smaller kinetic energy [1–3].

The above naive expectation motivates us to explore possible bound states composed of charmed (or bottomed) baryons $Y_{c(b)}$ ($\Lambda_{c(b)}$, $\Sigma_{c(b)}$, ...) and the nucleon (N) or nucleus. This is, of course, a natural extension of the hypernucleus, which is a nuclear bound state with one or more strange baryons Y (Λ, Σ, Ξ ...). Hypernuclear spectroscopy in the last decades played a key role in analysing structures of hypernuclei and extracting information on the YN and YY interactions. Because there is no two-body bound states in ΛN or ΣN systems and it is difficult to perform direct scattering experiments for the hyperons, it is important to get information on their interactions from the three-body or heavier nucleus with strange baryon(s).

Channels	1	2	3	4	5	6	7
$J^\pi = 0^+$	$\Lambda_c N(^1S_0)$	$\Sigma_c N(^1S_0)$	$\Sigma_c^* N(^5D_0)$				
$J^\pi = 1^+$	$\Lambda_c N(^3S_1)$	$\Sigma_c N(^3S_1)$	$\Sigma_c^* N(^3S_1)$	$\Lambda_c N(^3D_1)$	$\Sigma_c N(^3D_1)$	$\Sigma_c^* N(^3D_1)$	$\Sigma_c^* N(^5D_1)$

Table 1 The S-wave $\Lambda_c N$ states and the channels coupling to them [9]

The idea of the charmed hypernucleus is, in fact, old [4–11]. It was pointed out [6] that the SU(4) symmetry, though it is badly broken, for the one boson exchange (OBE) models predicts a weaker attraction between Y_c and N, because the K exchange is replaced by the D exchange, which is suppressed by the heavier mass of the D meson. Recent re-analysis with a model based on the heavy quark effective theories suggested the possibility of bound $Y_c N$ states. However, the model has a difficulty in describing the short-range interaction and its prediction was very sensitive to the cutoff parameters in the one-boson exchange interaction [9].

In this paper, we construct a potential model consisting of the long-range one-pion and one-sigma exchange interaction and the quark exchange effect based on the quark cluster model for the baryon-baryon interaction [12, 13]. The latter provides a short range repulsion between Y_c and N. Here Y_c represents Λ_c, Σ_c and Σ_c^*. The model also contains the off-diagonal components, which couple $\Lambda_c N$, $\Sigma_c N$ and $\Sigma_c^* N$ channels of the same total quantum numbers. By adjusting the meson exchange parameters to reproduce low-energy data of the NN system, we obtain four sets of the $Y_c N$ potential.

We solve the coupled channel Schrödinger equation using the Gaussian expansion method (GEM) [14] and obtain $\Lambda_c N$ bound states. The potential is also applied to the three-body $\Lambda_c NN$ system. Bound state solutions are found and their properties are analysed.

The paper is organized as follows. In Sec. 2, we present our model of the $Y_c N$ potential and explain how to determine the model parameters. In Sec. 3, the two-body $Y_c N$ systems are analysed with the obtained potentials and the results are examined. In Sec. 4, we construct an effective one-channel $\Lambda_c N$ potential model and apply it to the three-body $\Lambda_c NN$ system. Conclusions are given in Sec. 5.

2. Model of $Y_c N$ interactions

We first consider the two-baryon systems, with isospin $I = \frac{1}{2}$ and spin-parity $J^\pi = 0^+$ or 1^+. Table 1 shows possible channels contributed by $\Lambda_c N$, $\Sigma_c N$, and $\Sigma_c^* N$ for each J. The channels with the orbital angular momentum $L = 0$ and 2 will be coupled by tensor force, while those with the same L are coupled mainly by central force. We solve coupled channel Schrödinger equation in a hybrid potential model. The model includes a pion exchange potential and a scalar meson exchange potential for long-range interactions [9] and a short-range repulsive potential coming from the quark exchanges between the baryons [12].

2.1. One boson exchange potential

The meson exchange part contains four kinds of terms: spin-independent, spin-spin, spin-orbit, and tensor,

$$\begin{aligned} V_\pi(i,j) &= C_\pi(i,j)\frac{m_\pi^3}{24\pi f_\pi^2}\left\{\langle \boldsymbol{\mathcal{O}}_{spin}\rangle_{ij}\, Y_1(m_\pi,\Lambda_\pi,r) + \langle \boldsymbol{\mathcal{O}}_{ten}\rangle_{ij}\, H_3(m_\pi,\Lambda_\pi,r)\right\} \\ V_\sigma(i,j) &= C_\sigma(i,j)\frac{m_\sigma}{16\pi}\left\{\langle \mathbf{1}\rangle_{ij}\, 4Y_1(m_\sigma,\Lambda_\sigma,r) + \langle \boldsymbol{\mathcal{O}}_{LS}\rangle_{ij}\left(\frac{m_\sigma}{M_N}\right)^2 Z_3(m_\sigma,\Lambda_\sigma,r)\right\} \end{aligned} \tag{1}$$

where i and j are the labels of the channels and $C_\pi(i,j)$ and $C_\sigma(i,j)$ are the relevant coupling constants including the isospin factor. The spin dependent operators, $\boldsymbol{\mathcal{O}}_{spin}$, $\boldsymbol{\mathcal{O}}_{ten}$, and $\boldsymbol{\mathcal{O}}_{LS}$, and their expectation values are given in Appendix A. The r-dependent functions Y_1, H_3, and Z_3 contain the cutoff parameters Λ_π and Λ_σ. The explicit forms of the functions are given in Appendix B. We will determine the coupling strength and the cutoff parameters later.

2.2. Short range repulsion from Quark Cluster Model

In a previous approach [9], we considered exchanges of the vector mesons for the short range part of the Y_cN interaction. They, however, do not provide enough repulsion at short distances and result in very deep bound states with compact wave functions. As the wave function of the baryons overlap significantly at short distances, the quark exchange effect becomes important. We here employ the quark cluster model (QCM) for the short-range potential [12].

In QCM each baryon is a cluster determined made of three quarks. When the two clusters overlap at small r, the antisymmetrization among the (light) quarks induces a non-local interaction. When the two baryons overlap completely i.e., $r = 0$, all the six quarks occupy the lowest energy orbit with a single center. Such a state is approximately given by a product of the Gaussian wave functions with an appropriate symmetry according to the quantum numbers. The strength of the repulsive potential at $r = 0$ (V_0) is thus determined by the difference between the energy of the single-centered six-quark states and that of the individual baryons.

$$V_0 \approx \langle 6q|H|6q\rangle - 2\langle 3q|H|3q\rangle \tag{2}$$

It turns out [12] that the strengths are sensitive to and determined dominantly by the color-magnetic interaction (CMI) given by

$$V_{CM} = -\beta\sum_{i<j}(\boldsymbol{\sigma}_i\cdot\boldsymbol{\sigma}_j)(\boldsymbol{\lambda}_i\cdot\boldsymbol{\lambda}_j) \tag{3}$$

where $\boldsymbol{\sigma}_i$ and $\boldsymbol{\lambda}_i$ are the spin and color operators of the i-th quark. The expectation values of the color-magnetic operator for a five light quark systems can be computed by using the formula,

$$\langle V_{CM}\rangle = \beta\left[8N + \frac{4}{3}S(S+1) + 2C_2\left[SU(3)_c\right] - 4C_2\left[SU(6)_{cs}\right]\right], \tag{4}$$

where N is total number of light quarks, S is the total spin, and $C_2\,[SU(g)]$ is the quadratic Casimir operator, whose value is specified by the Young diagram $[f_1, \ldots, f_g]$,

$$C_2\,[SU(g)] = \frac{1}{2}\left[\sum_i f_i(f_i - 2i + g + 1) - \frac{N^2}{g}\right]. \tag{5}$$

The overall strength β can be determined by the $\Delta(1232)$ - nucleon (N) mass splitting, which comes also from V_{CM}. From $\langle V_{CM}\rangle_\Delta - \langle V_{CM}\rangle_N = -16\beta = 293$ MeV (exp.), we obtain $\beta \cong 18.2$ MeV. Table 2 shows the values of V_{CM} for various two-baryon (six-quark) states. These values are evaluated in the heavy quark limit, so that the heavy quark spin does not contribute.

System	V_0 [MeV]
$(NN)^{S=0}_{I=1}$	450
$(NN)^{S=1}_{I=0}$	350
$(\Lambda_c N)^{S=0}_{I=1/2}$	300
$(\Lambda_c N)^{S=1}_{I=1/2}$	300

$$\begin{pmatrix} \Sigma_c N \\ \Sigma_c^* N \end{pmatrix}^{S=0}_{I=1/2} = \begin{pmatrix} 100 & 0 \\ 0 & 0 \end{pmatrix}, \quad \begin{pmatrix} \Sigma_c N \\ \Sigma_c^* N \end{pmatrix}^{S=1}_{I=1/2} = \begin{pmatrix} 166.7 & -24.0 \\ -24.0 & 108.3 \end{pmatrix}$$

Table 2 Expectation values in MeV of the color magnetic interaction (CMI) for the relevant channels in the heavy quark limit. For the correlated channels of $\Sigma_c N$ and $\Sigma_c^* N$, the values are given in the matrix form.

We assume, for simplicity, that the radial dependence of the QCM potential is given by a Gaussian,

$$V_{QCM} = V_0 e^{-(r^2/b^2)}. \tag{6}$$

The range parameter b is supposed to coincide with the extension of the quark wave functions in the baryon. According to [13], the typical values for the NN interaction are about 0.54 $\sim$ 0.58 fm. For the $Y_c N$ systems, we use two typical values, $b = 0.5$ and 0.6 fm, and compute the results.

2.3. Coulomb potential

We also include the Coulomb potential between the charged baryons. In this calculation, we consider only the two-baryon channels coupling to $\Lambda_c N(I = \frac{1}{2})$. For the $\Lambda_c n$ system (total charge $Q = +1$), there is no Coulomb effect. For the $Q = 2$ channels, $\Lambda_c p$, $\Sigma_c^+ p$ and $\Sigma_c^{++} n$, we assume that the mixing of $\Sigma_c^+ p$ and $\Sigma_c^{++} n$ is not modified by the Coulomb interaction and make an approximation for the Coulomb potential with the combination,

$$\left|(\Sigma_c N)_{I=\frac{1}{2},I_3=+\frac{1}{2}}\right\rangle = -\sqrt{\frac{1}{3}}\left|\Sigma_c^+ p\right\rangle + \sqrt{\frac{2}{3}}\left|\Sigma_c^{++} n\right\rangle \tag{7}$$

Then the "effective" Coulomb potentials for the Y_cN channels are given by

$$V^{\Lambda_c N}_{coulomb}(r) = \frac{\alpha\hbar c}{r},$$
$$V^{\Sigma_c N}_{coulomb}(r) = \frac{1}{3}\frac{\alpha\hbar c}{r},$$
$$V^{\Sigma^*_c N}_{coulomb}(r) = \frac{1}{3}\frac{\alpha\hbar c}{r}, \tag{8}$$

where $\alpha \sim 1/137$ is the fine structure constant.

2.4. Determining the potential parameters

OBE=one bosom exchange

per lo scambio si usano i mesoni (sono quelli con quark pari) leggeri come i \pi e \sigma che mediano la forza nucleare

In the previous study using the OBE potential [9], we found that the results are very sensitive to the cutoff parameters. To remedy this problem, in the present approach, we adjust the parameters of the potential to reproduce the NN interaction data using the same model. In doing so, we fix the π-baryon coupling constants and the short-range potential derived from the quark model. Then the cutoffs, Λ_π and Λ_σ, and the sigma coupling constant, C_σ, are the parameters to be determined in the NN system. After that the results are generalized to the Y_cN system. In this method, we assume that the light mesons couple only to the light quarks and the cutoff parameters are common to NN and Y_cN systems. The details are given in Appendix B.

i parametri di cutoff indicano fino a che punto rimane valido quel potenziale

In searching the three undetermined parameters, Λ_π, Λ_σ and C_σ, we use the following experimental values of the NN interaction,

$$NN(^1S_0) \text{ scattering length} = -23.7\text{fm},$$
$$NN(^3S_1) \text{ binding energy(deuteron)} = 2.22\text{MeV}. \tag{9}$$

To get appropriate values, we restrict the possible range of parameters to be

$$\Lambda_\pi = 500 \sim 900\text{MeV},$$
$$\Lambda_\sigma = 900 \sim 1200\text{MeV},$$
$$C_\sigma(NN) = -64.0 \sim -225.0. \tag{10}$$

Unfortunately, we could not find a solution. Therefore we relax the condition that C_σ is independent of J^π and take $C_\sigma(J^\pi = 0^+)$ and $C_\sigma(J^\pi = 1^+)$ independently. Then we find solutions, which are given in Tables 3 and 4. In Table 3, we show parameters with a fixed $\Lambda_\pi = 750$ MeV and varied Λ_σ while Table 4 lists the results with varied Λ_π for a fixed $\Lambda_\sigma = 1000$ MeV. These two Tables also present the differences between $C_\sigma(J^\pi = 0^+)$ and $C_\sigma(J^\pi = 1^+)$,

$$\Delta_C = |C_\sigma(J^\pi = 0^+) - C_\sigma(J^\pi = 1^+)|. \tag{11}$$

QCM=quark cluster model

From the results in the Tables, one finds that Δ_C is insensitive to the change of Λ_σ, but Δ_C increases rapidly for increasing Λ_π. The features for $b = 0.5$ fm and 0.6 fm are qualitatively similar. Since the QCM repulsion for $b = 0.5$ fm is weaker than that for $b = 0.6$ fm, the resulting C_σ is also smaller and Δ_C tends to be smaller for $b = 0.5$ fm. We suppose that the spin dependence of C_σ is small, so that a small Δ_C is favoured.

The resulting NN potentials for $J^\pi = 0^+$ with the obtained parameters are plotted in Figs. 1 and 2. We find that some of the potentials (for small Λ_π) are strongly attractive

	$b = 0.6$[fm]			$b = 0.5$[fm]		
Λ_σ[MeV]	$C_\sigma(0^+)$	$C_\sigma(1^+)$	Δ_C	$C_\sigma(0^+)$	$C_\sigma(1^+)$	Δ_C
900	-213.16	-161.29	51.87	-176.89	-132.25	44.64
950	-179.56	-134.56	45.0	-148.84	-110.25	38.59
1000	-156.25	-118.81	37.44	-129.96	-96.04	33.92
1050	-141.61	-106.09	35.52	-116.64	-86.49	30.15
1100	-127.69	-96.04	31.65	-106.09	-79.21	26.88
1150	-116.64	-88.36	28.28	-98.01	-72.25	25.76
1200	-108.16	-82.81	25.35	-90.25	-67.24	23.01

Table 3 The NN 2-body parameters for $\Lambda_\pi = 750$ MeV

	$b = 0.6$[fm]			$b = 0.5$[fm]		
Λ_π[MeV]	$C_\sigma(0^+)$	$C_\sigma(1^+)$	Δ_C	$C_\sigma(0^+)$	$C_\sigma(1^+)$	Δ_C
500	-148.84	-139.24	9.6	-118.81	-121.0	2.19
550	-151.29	-136.89	14.4	-123.21	-116.64	6.57
600	-153.76	-134.56	19.2	-125.44	-114.49	10.95
650	-153.76	-129.96	23.8	-127.69	-110.25	17.44
700	-156.25	-125.44	30.81	-127.69	-104.04	23.65
750	-156.25	-118.81	37.44	-129.96	-96.04	33.92
800	-156.25	-110.25	48.51	-129.96	-88.36	41.6
850	-156.25	-102.01	54.24	-132.25	-79.21	53.04
900	-156.25	-92.16	66.6	-132.25	-70.56	61.69

Table 4 The NN 2-body parameters for $\Lambda_\sigma = 1000$ MeV

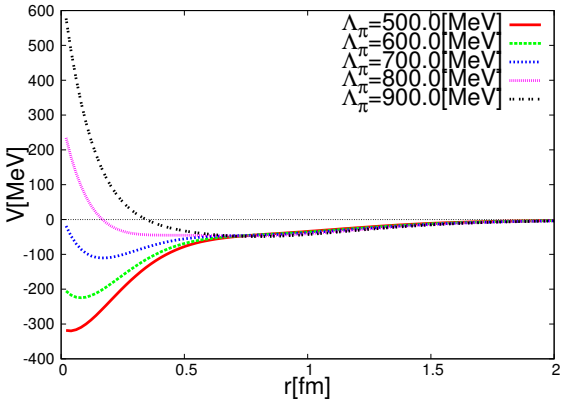

Fig. 1 NN potential ($J^\pi = 0^+$) for b=0.6fm and $\Lambda_\sigma = 1000$ MeV.

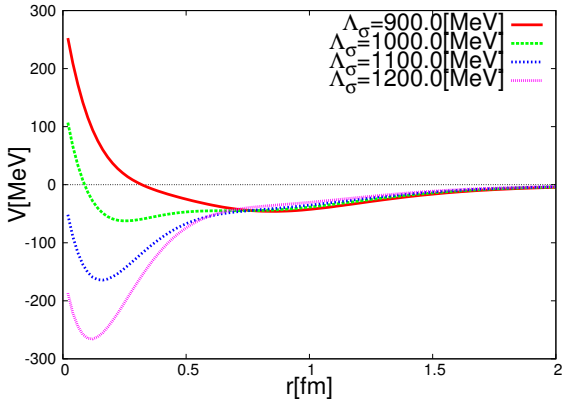

Fig. 2 NN potential ($J^\pi = 0^+$) for b=0.6fm and $\Lambda_\pi = 750$ MeV.

at short distances and may not be appropriate for the current purpose, although they all reproduce the $^1S_0$ scattering length and the deuteron binding energy.

Therefore we choose the parameters with $\Lambda_\pi = 750$ MeV and $\Lambda_\sigma = 1000$ MeV and employ four sets of the most realistic potential parameters, given in Table 5. We call these models

"CTNN" potentials, as these parameter sets correspond to the NN experimental data. The Y_cN potentials derived for $J^\pi = 0^+$ are shown in Figs. 3 - 8. In Appendix C, we show the Y_cN potentials for $J^\pi = 1^+$ and also the individual components of the CTNN-a potential.

	C_σ	b[fm]
parameter a	-67.58	0.6
parameter b	-77.5	0.6
parameter c	-60.76	0.5
parameter d	-70.68	0.5

Table 5 The CTNN potential parameters

3. Y_cN bound states

In solving the Schrödinger equation for the two-baryon system, we employ a variational method with Gaussian trial functions, the Gaussian Expansion Method [14], where the radial wave functions are expanded by the basis states given by Gaussian functions with varied range parameters.

$$\begin{aligned}\psi_{lm}(\boldsymbol{r}) &= \sum_{n=1}^{n_{max}} c_{nl}\phi^G_{nlm}(\boldsymbol{r}) \\ \phi^G_{nlm}(\boldsymbol{r}) &= \phi^G_{nl}(r)Y_{lm}(\hat{\boldsymbol{r}}) \\ \phi^G_{nl}(r) &= N_{nl}r^l e^{-\nu_n r^2} \\ \nu_n &= \frac{1}{r_n} = \frac{1}{r_1 a^{n-1}}\end{aligned} \tag{12}$$

This method has been applied to various bound state problems and was proved to give an accurate approximation to the eigenstate-energies and wave functions.

The Y_cN binding energies are given in Tables 6 and 7. The $\Lambda_c n$ system ($J^\pi = 0^+$ or 1^+) without the Coulomb potential has a bound state for the Y_cN-CTNN parameter b, c, and d. The CTNN-b and c potentials allow very shallow bound states and the CTNN-d potential gives a larger binding energy. The result indicates that there is a strong QCM repulsion at short distances for the CTNN-a and b parameters. On the other hand, the $\Lambda_c p$ system with the Coulomb potential has a bound state only for the parameter CTNN-d.

As a cross check, we also calculate the $\Lambda_c N$ scattering lengths for the CTNN potentials. These results are consistent with the binding energies (see Tables 6 and 7.)

The above results show that the binding energies of the $J^\pi = 1^+$ states are larger than those of $J^\pi = 0^+$. This is consistent with the previous study [9].

Table 7 also shows the probabilities of the coupled channels. For all the parameter sets and the total angular momenta, the probability of $\Lambda_c N$ is more than 99 % . In the case of $J^\pi = 0^+$, the probabilities of $\Sigma_c^* N$ ($^5D_0$) are larger than that of $\Sigma_c N$ ($^1S_0$). On the other hand, in the case of $J^\pi = 1^+$, the respective total probabilities of $\Sigma_c N$ and $\Sigma_c^* N$ are almost equal. Looking closely, $\Sigma_c N(^3S_1)$ and $\Sigma_c^* N(^5D_1)$ contribute largely to the results. These observations can be explained with the contributions of the strong tensor force between the $\Lambda_c N$ ($L = 0$) and $\Sigma_c N$ / $\Sigma_c^* N$ ($L = 2$) channels.

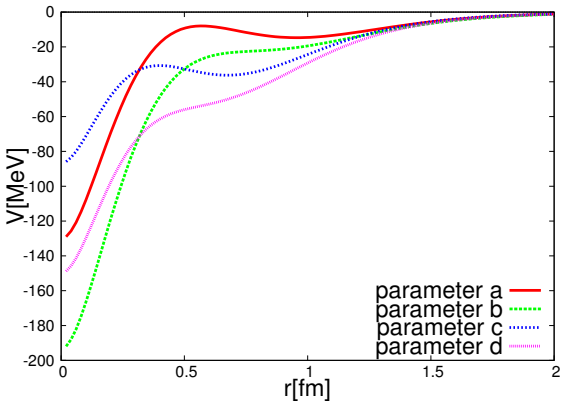

Fig. 3 Y_cN-CTNN potential for the Λ_cN single channel.

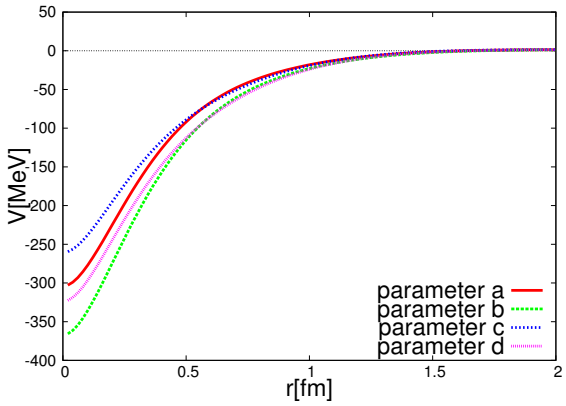

Fig. 4 Y_cN-CTNN potential for the Σ_cN single channel.

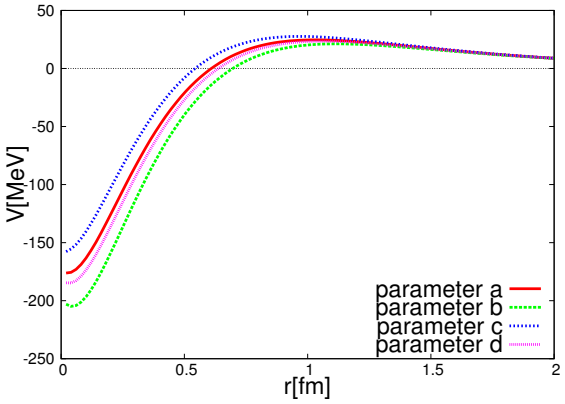

Fig. 5 Y_cN-CTNN potential for the Σ_c^*N single channel.

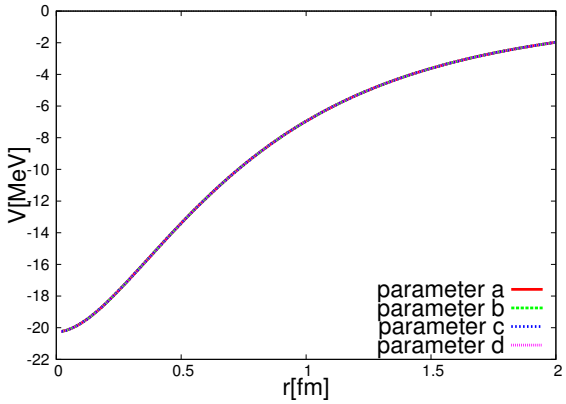

Fig. 6 Y_cN-CTNN potential for the Λ_cN-Σ_cN channels.

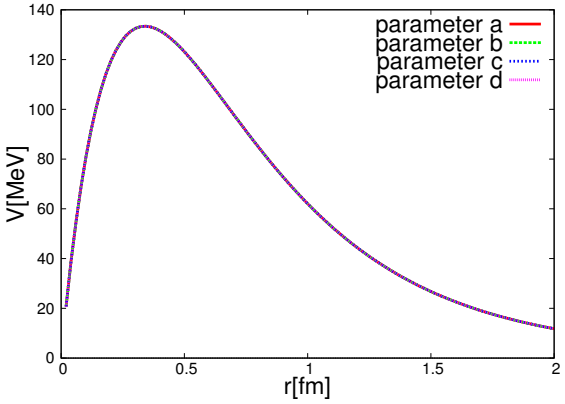

Fig. 7 Y_cN-CTNN potential for the Λ_cN-Σ_c^*N channels.

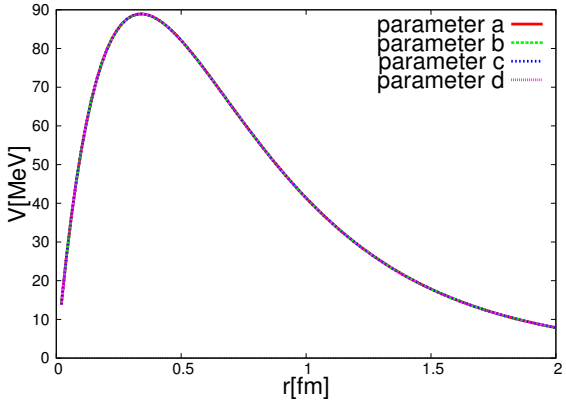

Fig. 8 Y_cN-CTNN potential for the Σ_cN-Σ_c^*N channels.

4. Λ_cNN systems questo direi che non fa per me io ho un solo nucleone

4.1. Effects of channel couplings

In the previous section, we find that the probabilities of the Λ_cN component are almost 100% and the mixings of Σ_cN or Σ_c^*N are small. However, effects of the $\Sigma_cN - \Sigma_c^*N$ channel

$J^\pi = 0^+$	CTNN-a	CTNN-b	CTNN-c	CTNN-d
B.E. [MeV]	-	-	1.72×10^{-3}	1.37
(+ Coulomb)				(0.56)
scattering length [fm]	-3.64	-65.15	130.93	5.31
probability($\Lambda_c N$)[%]	-	-	99.97	99.29
probability($\Sigma_c N$)[%]	-	-	7.0×10^{-3}	0.20
probability($\Sigma_c^* N$)[%]	-	-	2.1×10^{-2}	0.51

Table 6 Binding energies of $\Lambda_c N$ ($J^\pi = 0^+$) for the CTNN potentials. The probabilities of the $\Sigma_c N$ and $\Sigma_c^* N$ channels are also shown.

$J^\pi = 1^+$	CTNN-a	CTNN-b	CTNN-c	CTNN-d
B.E. [MeV]	-	1.67×10^{-4}	1.91×10^{-2}	1.56
(+ Coulomb)				(0.72)
scattering length [fm]	-4.11	337.53	39.27	5.01
probability($\Lambda_c N$)[%]	-	99.99	99.90	99.23
probability($\Sigma_c N$)[%]	-	4.9×10^{-3}	4.9×10^{-2}	0.39
(D-wave ($^3D_1$))	-	4.5×10^{-3}	4.6×10^{-2}	0.35
probability($\Sigma_c^* N$)[%]	-	4.6×10^{-3}	4.6×10^{-2}	0.38
(D-wave ($^5D_1$))	-	3.1×10^{-3}	3.2×10^{-2}	0.25

Table 7 Binding energies of $\Lambda_c N$ ($J^\pi = 1^+$) for the CTNN potentials. The probabilities of the coupled D-wave $\Lambda_c N$ and $\Sigma_c N$ and $\Sigma_c^* N$ channels are also shown.

	$\Lambda_c N - \Sigma_c N - \Sigma_c^* N$		$\Lambda_c N$		$\Lambda_c N - \Sigma_c N$		$\Lambda_c N - \Sigma_c^* N$	
J^π	0^+	1^+	0^+	1^+	0^+	1^+	0^+	1^+
CTNN-a	-3.63	-4.10	-1.11	-1.11	-1.16	-2.07	-3.13	-2.09
CTNN-b	-63.25	398.67	-2.62	-2.62	-2.78	–6.74	-20.84	-7.00
CTNN-c	139.07	39.96	-3.01	-3.01	-3.19	-8.61	-48.56	-9.00
CTNN-d	5.32	5.02	-28.59	-28.59	-44.65	9.79	6.01	9.36
B.E.	1.37	1.56	-	-	-	0.36	1.04	0.39

Table 8 Scattering lengths in fm, and two-body binding energies in MeV for the cases that the coupled channels are reduced to $\Lambda_c N$ only, $\Lambda_c N$-$\Sigma_c N$ or $\Lambda_c N$-$\Sigma_c^* N$

coupling are important in binding the $\Lambda_c N$ system, because the single channel calculations of $\Lambda_c N$ do not show any binding solutions for all the CTNN-a $\sim$ d potentials.

In Table 8, we show the scattering lengths obtained for partially coupled systems, i.e., $\Lambda_c N$, $\Lambda_c N - \Sigma_c N$, and $\Lambda_c N - \Sigma_c^* N$. It is found that only the CTNN-d potential allows bound states in the $\Lambda_c N - \Sigma_c^* N$ (0^+ and 1^+) and the $\Lambda_c N - \Sigma_c N$ (1^+) systems. In particular, effect of the $\Sigma_c^* N$ (0^+) channel is large because no bound state is found without this channel. This indicates that the tensor force from the one-pion exchange, which induces the coupling between $\Sigma_c^* N$ ($^5D_0$) and $\Lambda_c N$ ($^1S_0$), is significant. Similarly, the contributions of the tensor force and $\Sigma_c N - \Sigma_c^* N$ couplings are found to be important for the $J^\pi = 1^+$ state.

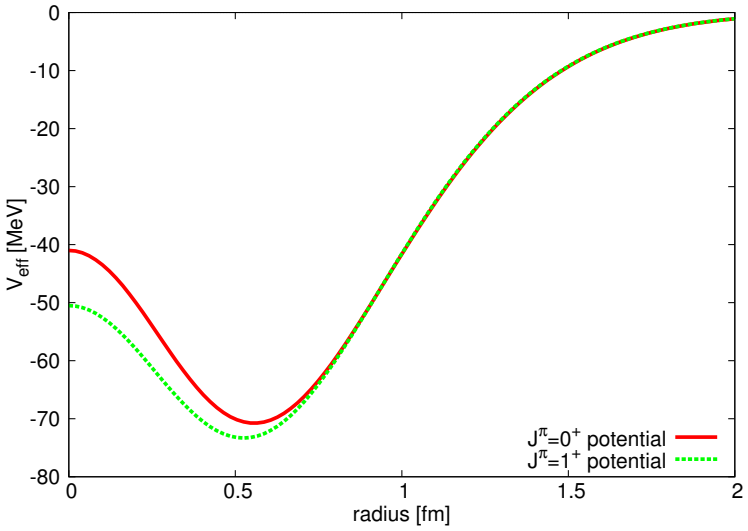

Fig. 9 $\Lambda_c N$ effective potentials for $J^\pi = 0^+$ and 1^+.

4.2. Effective $\Lambda_c N$ potential

In order to apply the obtained potentials to many-body systems with Λ_c, we construct effective single-channel $\Lambda_c N$ potentials, in which the effects of the $\Sigma_c N - \Sigma_c^* N$ couplings are absorbed in phenomenological parameters. We assume two-range Gaussian forms,

$$V_{\rm eff}^{0+} = V_1^{0+} e^{-\frac{r^2}{b_1^2}} + V_2^{0+} e^{-\frac{r^2}{b_2^2}}.$$
$$V_{\rm eff}^{1+} = V_1^{1+} e^{-\frac{r^2}{b_1^2}} + V_2^{1+} e^{-\frac{r^2}{b_2^2}}. \quad (13)$$

Here, b_1 and b_2 are range parameters, and V_1^{JP} and V_2^{JP} are the strength parameters. They are determined from the CTNN potentials. For simplicity, we choose the same b_1 and b_2 for $J^\pi = 0^+$ and 1^+, and rewrite Eq. (13) to be

$$V_{{\rm eff}_{Y_c N}} = \left[V_r^1 + \boldsymbol{\sigma}_{\Lambda_c} \cdot \boldsymbol{\sigma} V_s^1\right] e^{-\frac{r^2}{b_1^2}} + \left[V_r^2 + \boldsymbol{\sigma}_{\Lambda_c} \cdot \boldsymbol{\sigma} V_s^2\right] e^{-\frac{r^2}{b_2^2}}, \quad (14)$$

$$\begin{aligned} V_r^i &= \tfrac{1}{4}(V_i^{0+} + 3V_i^{1+}), \\ V_s^i &= \tfrac{1}{4}(V_i^{1+} - V_i^{0+}). \end{aligned} \quad (15)$$

Now, we use only the CTNN-d $Y_c N$ potential to construct the effective one. By reproducing the binding energies and the scattering lengths in Tables 6 and 7, we search values of the parameters, in Eq. (13). In doing so, we assume that the first term (V_1 of Eq. (13)) is an attractive potential like OBEP and the second term (V_2) is repulsive like the QCM repulsion. Accordingly, b_2 is taken to be the radius of the quark wave function, $b_2 = 0.5$fm. On the other hand, $b_1 = 0.9$ fm is chosen to represent a typical range of the meson exchange potential which couples $\Sigma_c N$ and $\Sigma_c^* N$ to $\Lambda_c N$.

The remaining parameters of the effective potential are chosen as

$$V_1^{0+} = -150.0[\text{MeV}],\ V_2^{0+} = 109.0[\text{MeV}],\ V_1^{1+} = -149.0[\text{MeV}],\ V_2^{1+} = 98.5[\text{MeV}]. \quad (16)$$

Fig. 9 illustrates the shape of the effective potentials.

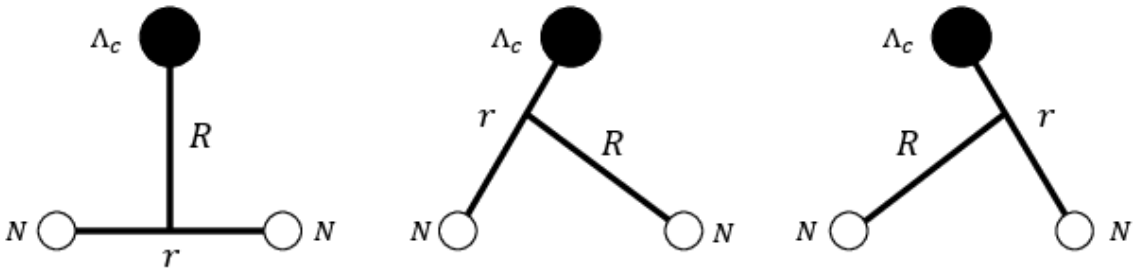

Fig. 10 Jacobi coordinates for $\Lambda_c NN$ system.

Alternatively, one can express the effective potential with the strengths of the spin-independent terms and the spin-spin terms,

$$V_r^1 = -149.25[\mathrm{MeV}],\ \mathrm{V_s^1} = 0.25[\mathrm{MeV}],\ \mathrm{V_r^2} = 101.125[\mathrm{MeV}],\ \mathrm{V_s^2} = -2.625[\mathrm{MeV}]. \quad (17)$$

It is obvious that the spin dependent potential is weak. This is a consequence of the heavy quark spin symmetry [20–23].

4.3. $\Lambda_c NN$ bound states

anche questo direi che...

Next, we study the $\Lambda_c NN$ three-body system by using the above $\Lambda_c N$ effective potential. In the calculation, we adopt the Jacobi coordinates shown in Fig. 10. The angular momenta, l and L are defined corresponding to r and R, respectively. On the other hand, we define the spin for two nucleons as S_{NN}, and the total spin of the systems as S_{tot}. For the isoscalar case, the binding energy is calculated from the threshold of Λ_c plus the deuteron, while for the case $I = 1$, the calculation is from the threshold of the bound $\Lambda_c N$ (binding energy=1.56 MeV) plus a nucleon.

In this study, we assume that the orbital angular momenta, l and L, are both zero. Then S_{NN} and I are related and possible J^π are

$$\begin{array}{lll} I=0 & \cdots & S_{NN}=1,\ \ J^\pi = \frac{1}{2} \text{ or } \frac{3}{2}, \\ I=1 & \cdots & S_{NN}=0,\ \ J^\pi = \frac{1}{2}. \end{array} \quad (18)$$

There are various potential models for the NN system [15–19]. Here we employ the Minnesota potential [15]. It describes the deuteron only with S-wave component, as the D-wave contribution is effectively included in the central potential,

$$V_{ij}(r) = \left(V_R + \frac{1}{2}(1+P_{ij}^\sigma)V_t + \frac{1}{2}(1-P_{ij}^\sigma)V_s\right)\left(\frac{1}{2}u + \frac{1}{2}(2-u)P_{ij}^r\right) \quad (19)$$

$$V_R(r) = V_{0R}e^{-\kappa_R r^2},\ V_t(r) = V_{0t}e^{-\kappa_t r^2},\ V_s(r) = V_{0s}e^{-\kappa_s r^2} \quad (20)$$

$$\begin{aligned} V_{0R} &= 200.0[\mathrm{MeV}],\ \kappa_R = 1.487[\mathrm{fm}^{-2}], \\ V_{0t} &= -178.0[\mathrm{MeV}],\ \kappa_t = 0.639[\mathrm{fm}^{-2}], \\ V_{0s} &= -91.85[\mathrm{MeV}],\ \kappa_s = 0.465[\mathrm{fm}^{-2}]. \end{aligned} \quad (21)$$

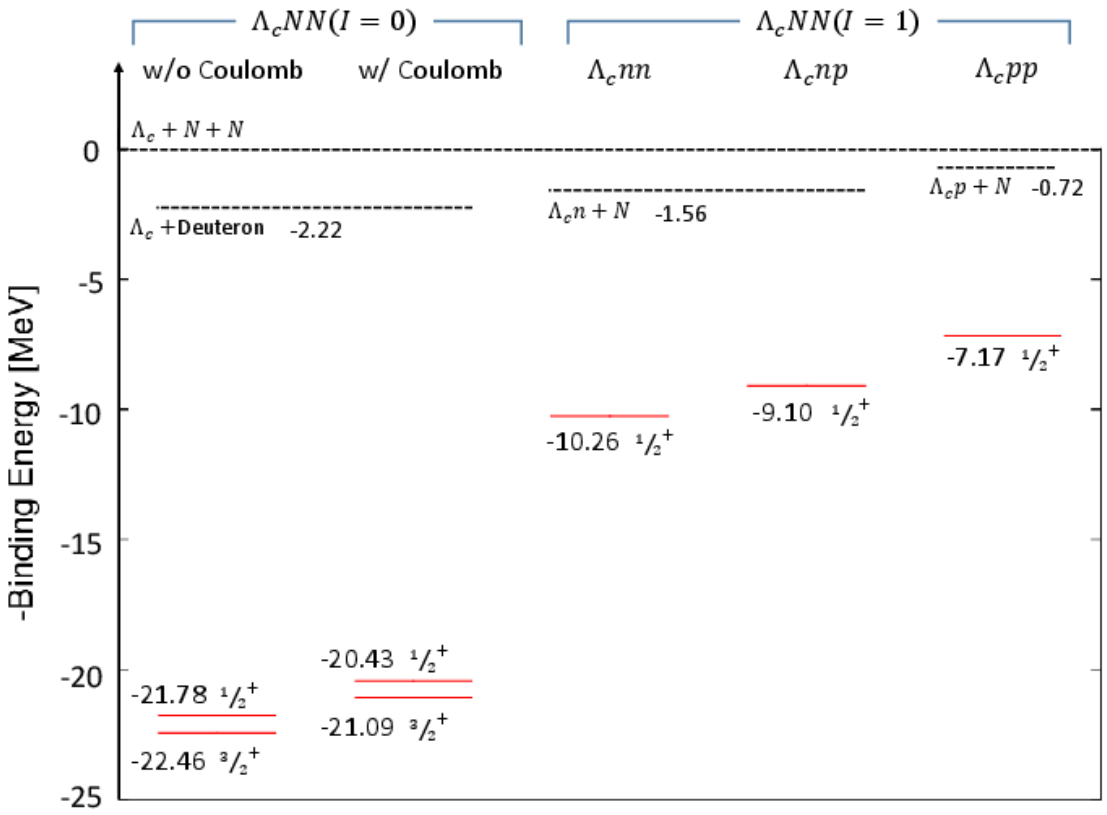

Fig. 11 $\Lambda_c NN$ binding energies. The dotted lines are the Λ_c-deuteron threshold that is 2.22 MeV below the $\Lambda_c NN$ threshold, the threshold of the $(\Lambda_c n)$ 1^+ bound state plus a nucleon, i.e., 1.56 MeV below $\Lambda_c NN$, and the threshold of the $(\Lambda_c p)$ 1^+ bound state plus a nucleon, i.e., 0.72 MeV below $\Lambda_c NN$

We again use GEM [14] to solve the three-body problem. The binding energies of the $\Lambda_c NN$ three-body system with the $\Lambda_c N$ effective potential are shown in Fig. 11. The left two plots show the results for $I = 0$ without and with the Coulomb potential, respectively. The others represent the $I = 1$ results for $\Lambda_c nn$, $\Lambda_c np$, and $\Lambda_c pp$. For each system, we find a bound state. Because the spin-spin interaction between Λ_c and N is weak (Table 7), the binding energies of $J^\pi = \frac{1}{2}^+$ and $\frac{3}{2}^+$ are close to each other for the case of $I = 0$. These results agree well with the heavy quark spin symmetry [20]. In the present calculation, we find that the $\frac{3}{2}^+$ state is lower in energy than the $\frac{1}{2}^+$ state by about 0.7 MeV. These results are consistent with a recent three-body calculation [10], which also favors the $\frac{3}{2}^+$ $\Lambda_c NN$ as the lowest state. Effect of the Coulomb potential between Λ_c and proton is smaller than the difference between the $I = 0$ and 1 results.

Tables 9 and 10 show the mean distances in the bound state, where r is the root mean square (rms) distance between the nucleons, and R is rms distance between Λ_c and the center

	Binding energy [MeV]	(From threshold)	r [fm]	R [fm]
$\Lambda_c np$ w/o Coulomb $J^\pi = \frac{1}{2}^+$	21.78	19.56	1.91	1.34
$\Lambda_c np$ w/o Coulomb $J^\pi = \frac{3}{2}^+$	22.46	20.24	1.90	1.32
$\Lambda_c np$ w/ Coulomb $J^\pi = \frac{1}{2}^+$	20.43	18.21	1.93	1.36
$\Lambda_c np$ w/ Coulomb $J^\pi = \frac{3}{2}^+$	21.09	18.87	1.91	1.34

Table 9 $\Lambda_c NN$ binding energies and particle distances for the $I = 0$ bound states

	Binding energy [MeV]	(From threshold)	r [fm]	R [fm]
$\Lambda_c nn$ $J^\pi = \frac{1}{2}^+$	10.26	8.70	2.62	1.64
$\Lambda_c np$ $J^\pi = \frac{1}{2}^+$	9.10	7.54	2.67	1.68
$\Lambda_c pp$ $J^\pi = \frac{1}{2}^+$	7.17	6.35	2.78	1.75

Table 10 $\Lambda_c NN$ binding energies and particle distances for the $I = 1$ bound states

of NN. These Tables illustrate that the mean NN separations, r's, are significantly smaller than the mean distance of $p - n$ in the deuteron, about 3.8 fm. Namely, the Λ_c attraction to the nucleon makes the $\Lambda_c NN$ system shrink. It is also observed that R is smaller than r. Thus we can draw an intuitive picture that the nucleons go around Λ_c sitting at the center in the $\Lambda_c NN$ system. This property is also seen in the hypernuclear system, but the attractive force in the charmed nuclear system is stronger than that in the hypernuclear system.

We may check whether these results depend on the choice of the NN potential. Here we have used the Minnesota potential, which is known to have a weak repulsive core. For comparison, we replace the Minnesota potential by the AV8′ potential [24] and apply it to the $I = 1$ $\Lambda_c nn$ system. For the $I = 0$ $\Lambda_c NN$ systems, the comparison is not appropriate because the AV8′ contains the tensor force which make the D-wave components couple.

Then we obtain the binding energy BE= 11.93 [MeV] and the rms distances as $r = 2.41$ [fm] and $R = 1.54$ [fm]. These results can be compared to the first line of Table 10. One sees that they are consistent with each other. Thus we conclude that the qualitative behavior of the $\Lambda_c NN$ bound state is independent of the choice of the NN potential.

5. Conclusion

We have examined the interactions between the ground-state charmed baryons Λ_c, Σ_c and Σ_c^* and the nucleon N. Potential models are proposed, which are composed of the long-range one-boson exchange (OBE) force and the short-range quark exchange force based on the quark cluster model (QCM). We also include the Coulomb potential between the charged baryons. The parameters in the model, the cutoffs and the coupling constant of σ meson, are determined so that the NN data are reproduced in the same model. By fitting the deuteron binding energy and the S-wave scattering lengths, four parameter sets are obtained.

We have applied these potentials to the two-body $\Lambda_c N - \Sigma_c N - \Sigma_c^* N$ coupled system. The coupled-channel Schrödinger equation is solved to a good precision by the Gaussian expansion method. We find shallow bound $\Lambda_c N$ states both in $J^\pi = 0^+$ and 1^+ in two of the four parameter sets. Those parameters are the cases that the ranges of the QCM

repulsion are small and thus the quark exchange effect is weaker than the other two. The difference between the $J^\pi = 0^+$ ($\Lambda_c N(^1S_0)$) and 1^+ ($\Lambda_c N(^3S_1)$) systems is small, which is a consequence of the heavy quark spin symmetry.

It is not surprising to have a bound state in these channels, because the $Y_c N$ interactions are similar to those of YN except for the K exchange part, while the kinetic energy is suppressed by the heavier mass. Furthermore, the effect of the channel coupling to $\Sigma_c^* N$ is significant due to the strong tensor force coming from the one-pion exchange. We then conclude that shallow $\Lambda_c N$ bound states may exist.

Encouraged by the possible existence of the two-body bound states, we further consider three-body $\Lambda_c NN$ bound states. This is the lightest "charmed nucleus", which corresponds to the hyper-triton (Λpn) bound state in the strangeness sector. In order to simplify the calculation, in the present approach, we first construct an effective one-channel ($\Lambda_c N$) potential from the fully coupled ($\Lambda_c N - \Sigma_c N - \Sigma_c^* N$) calculation. Using the effective one-channel potential, we have solved the three-body Schrödinger equation with the GEM and have obtained bound states with the binding energy about 20-22 MeV for $I = 0$, and 7-10 MeV for $I = 1$ from the $\Lambda_c NN$ threshold. The corresponding wave functions indicate that the Λ_c baryon makes the size of the NN system significantly smaller owing to attractive force. In order to confirm these results, further studies with the full and explicit couplings with the $\Sigma_c N$ and $\Sigma_c^* N$ channels will be necessary.

Acknowledgment

S. M. is supported by the RIKEN Junior Research Associate Program. This work is supported in part by JSPS KAKENHI Grant Nos. 25247036, and 24250294. Y. R. L. was supported by the "Program for Promoting the Enhancement of Research Universities "at Tokyo Institute of Technology in 2014 and partly by NNSFC(No. 11275115). This work is also supported by the Research Abroad and Invitational Program for the Promotion of International Joint Research, Category (C) and the International Physics Leadership Program at Tokyo Tech.

References

[1] D. Acosta et al. (CDF II Collaboration), Phys. Rev. Lett. 93, 072001 (2004).
[2] A. V. Manohar and M. B. Wise, Nucl. Phys. B **399** 17 (1993)
[3] S. Ohkoda, Y. Yamaguchi, S. Yasui, K. Sudoh, and A. Hosaka, Phys. Rev. D **86**, 034019 (2012)
[4] C.B. Dover and S.H. Kahana, Phys. Rev. Lett. **39**, 1506 (1977).
[5] G. Bhamathi, Phys. Rev. C **24**, 181 (1981).
[6] H. Bando and M. Bando, Phys. Lett. B **109**, 164 (1982); H. Bando and S. Nagata, Prog. Theor. Phys. **69**, 557 (1983); H. Bando, Prog. Theor. Phys. Suppl. **81**, 197 (1985).
[7] B.F. Gibson, C.B. Dover, G. Bhamathi, and D.R. Lehman, Phys. Rev. C **27**, 2085 (1983).
[8] Y.A. Batusov et al., JETP Lett. **33**, 56 (1981).
[9] Y. R. Liu, and M. Oka, Phys. Rev. D **85**, 014015 (2012).
[10] H. Garcilazo, A. Valcarce, and T.F. Carames, Phys. Rev. C **92** 024006 (2015).
[11] A. Gal, H. Garcilazo, A. Valcarce, and T. Fernandez-Carames, Phys. Rev. D **90**, 014019, (2014)
[12] M. Oka, and K. Yazaki, Phys. Lett. B **90**, 41 (1980); M. Oka, K. Shimizu, and K. Yazaki, Nucl. Phys. A **464** 700 (1987); M. Oka, K. Shimizu, and K. Yazaki, Prog. Theor. Phys. Suppl. **137** 1 (2000); M. Oka, Nucl. Phys. A, **881**, 6 (2012)
[13] S. Takeuchi, O. Morimatsu, Y. Tani and M. Oka, Prog. Theor. Phys. Suppl. **137**, 83 (2000).
[14] E. Hiyama, Y. Kino, and M. Kamimura, Prog. Part. Nucl. Phys. **51**, 223 (2003).
[15] D. R. Thompson, M. Lemere, and Y. C. Tang, Nuci. Phys. A **286**, 53 (1977).
[16] T. A. Rijken, M. M. Nagels and Y. Yamamoto, Prog. Theor. Phys. Suppl. **185**, 14 (2010).
[17] R. B. Wiringa, V. G. J. Stoks and R. Schiavilla, Phys. Rev. C **51**, 38 (1995).
[18] R. Machleidt, Phys. Rev. C **63**, 024001 (2001).
[19] R. Tamagaki, Prog. Theor. Phys. **39**, 91 (1967).
[20] N. Isgur and M.B. Wise, Phys. Lett. B **232**, 113 (1989).
[21] M. Oka, Y. R. Liu, and W. Meguro, Few Body Syst. **54**, 1255 (2013).
[22] S. Yasui, K. Sudoh, Y. Yamaguchi, S. Ohkoda, A. Hosaka, and T. Hyodo, Phys. Lett. B **727** 185 (2013).
[23] Y. Yamaguchi, S. Ohkoda, A. Hosaka, T. Hyodo, and S. Yasui, Phys. Rev. D **91** 034034 (2015).
[24] B. S. Pudliner, and V. R. Pandharipande, Phys. Rev. C **56**, 1720 (1997).
[25] K. Nakamura et al. (Particle Data Group), J. Phys. G **37** 075021 (2010).
[26] A. Manohar and H. Georgi, Nucl. Phys. B **234**, 189 (1984).
[27] D. Jido, M. Oka, and A. Hosaka, Prog. Theor. Phys. **106**, 873 (2001).
[28] S. Ishida et al., Prog. Thepr. Phys. **95**, 745 (1996).
[29] K. Igi and K.I. Hisaka, Phys. Rev. D **59**, 034005 (1999).
[30] G. Colangelo, J. Gasser, and H. Leutwyler, Nucl. Phys. B **603**, 125 (2001); I. Caprini, G. Colangelo, and H. Leutwyler, Phys. Rev. Lett. **96**, 132001 (2006).

Appendix A. Spin Matrix Elements of Y_cN OBE potential

In this Appendix, we present the definitions of the spin dependent operators in the potentials. $\boldsymbol{\mathcal{O}}_{spin}$ is the spin-spin operator between Y_c and N:

$$\boldsymbol{\mathcal{O}}_{spin} = \boldsymbol{\mathcal{O}}_1 \cdot \boldsymbol{\sigma}_2, \tag{A1}$$

where $\boldsymbol{\sigma}_2$ is the Pauli matrix of the nucleon spin, and $\boldsymbol{\mathcal{O}}_1$ is the spin operator of the charmed baryon,

$$\boldsymbol{\mathcal{O}}_1 = \begin{cases} \boldsymbol{\sigma}_1 & \text{for } \Lambda_\mathrm{c} \text{ and } \Sigma_\mathrm{c} \\ \bar{\boldsymbol{\Sigma}}_1 & \text{for the transition from } \Lambda_\mathrm{c} \text{ and } \Sigma_\mathrm{c} \text{ to } \Sigma_\mathrm{c}^* \\ \boldsymbol{\Sigma}_1 & \text{for } \Sigma_\mathrm{c}^* \end{cases} \tag{A2}$$

The transition spin $\bar{\boldsymbol{\Sigma}}$ is defined as $u^\mu \equiv \bar{\boldsymbol{\Sigma}}\Phi$, where u^μ is the Rarita Schwinger field, and Φ is the spin wave functions of Σ_c^*,

$$\Phi(3/2) = \begin{pmatrix} 1 \\ 0 \\ 0 \\ 0 \end{pmatrix},\ \Phi(1/2) = \begin{pmatrix} 0 \\ 1 \\ 0 \\ 0 \end{pmatrix},\ \Phi(-1/2) = \begin{pmatrix} 0 \\ 0 \\ 1 \\ 0 \end{pmatrix},\ \Phi(-3/2) = \begin{pmatrix} 0 \\ 0 \\ 0 \\ 1 \end{pmatrix}. \tag{A3}$$

Then we calculate the transition spin explicitly,

$$\begin{aligned} \bar{\boldsymbol{\Sigma}}^\dagger &= -\tfrac{1}{\sqrt{2}}\left(\bar{\boldsymbol{\Sigma}}_x^\dagger + i\bar{\boldsymbol{\Sigma}}_y^\dagger\right) + \tfrac{1}{\sqrt{2}}\left(\bar{\boldsymbol{\Sigma}}_x^\dagger - i\bar{\boldsymbol{\Sigma}}_y^\dagger\right) + \bar{\boldsymbol{\Sigma}}_z^\dagger \\ &= \begin{pmatrix} 1 & 0 & 0 & 0 \\ 0 & \sqrt{\frac{1}{3}} & 0 & 0 \end{pmatrix} + \begin{pmatrix} 0 & \sqrt{\frac{2}{3}} & 0 & 0 \\ 0 & 0 & \sqrt{\frac{2}{3}} & 0 \end{pmatrix} + \begin{pmatrix} 0 & 0 & \sqrt{\frac{1}{3}} & 0 \\ 0 & 0 & 0 & 1 \end{pmatrix} \end{aligned} \tag{A4}$$

$$\bar{\boldsymbol{\Sigma}}\bar{\boldsymbol{\Sigma}}^\dagger = -I_{4\times4}, \quad \bar{\boldsymbol{\Sigma}}^\dagger\bar{\boldsymbol{\Sigma}} = -2I_{2\times2}. \tag{A5}$$

With $\hat{\boldsymbol{e}}(\lambda=+1) = -\frac{1}{\sqrt{2}}(1,i,0)$, $\hat{\boldsymbol{e}}(\lambda=-1) = \frac{1}{\sqrt{2}}(1,-i,0)$, $\hat{\boldsymbol{e}}(\lambda=0) = (0,0,1)$, and $S_{t\mu}^\dagger = (0,\vec{S}_t^\dagger)$, one has

$$\bar{\boldsymbol{\Sigma}}(1,+1) = \begin{pmatrix} 1 & 0 \\ 0 & \sqrt{\frac{1}{3}} \\ 0 & 0 \\ 0 & 0 \end{pmatrix}, \qquad \bar{\boldsymbol{\Sigma}}(1,-1) = \begin{pmatrix} 0 & 0 \\ 0 & 0 \\ \sqrt{\frac{1}{3}} & 0 \\ 0 & 1 \end{pmatrix}, \qquad \bar{\boldsymbol{\Sigma}}(1,0) = \begin{pmatrix} 0 & 0 \\ \sqrt{\frac{2}{3}} & 0 \\ 0 & \sqrt{\frac{2}{3}} \\ 0 & 0 \end{pmatrix} \tag{A6}$$

Next, we define the spin operator of Σ_c^*,

$$\begin{aligned} \boldsymbol{\Sigma} = -S_{t\mu}^\dagger \boldsymbol{\sigma} S_t^\mu = (S_t^\dagger)^j \boldsymbol{\sigma} (S_t)^j, \\ \boldsymbol{S}(\Sigma_c^*) = \tfrac{3}{2}\boldsymbol{\Sigma}. \end{aligned} \tag{A7}$$

With Eq. (A6), the explicit matrices are

$$\begin{aligned}
\boldsymbol{\sigma}_{rs}(1,+1) &= -\tfrac{1}{\sqrt{2}}\left(\boldsymbol{\Sigma}_x + i\boldsymbol{\Sigma}_y\right) = -\begin{pmatrix} 0 & \sqrt{\frac{2}{3}} & 0 & 0 \\ 0 & 0 & \frac{2\sqrt{2}}{3} & 0 \\ 0 & 0 & 0 & \sqrt{\frac{2}{3}} \\ 0 & 0 & 0 & 0 \end{pmatrix}, \\
\boldsymbol{\sigma}_{rs}(1,-1) &= \tfrac{1}{\sqrt{2}}\left(\boldsymbol{\Sigma}_x - i\boldsymbol{\Sigma}_y\right) = -\begin{pmatrix} 0 & 0 & 0 & 0 \\ \sqrt{\frac{2}{3}} & 0 & 0 & 0 \\ 0 & \frac{2\sqrt{2}}{3} & 0 & 0 \\ 0 & 0 & \sqrt{\frac{2}{3}} & 0 \end{pmatrix}, \\
\boldsymbol{\sigma}_{rs}(1,0) &= \boldsymbol{\Sigma}_z = -\begin{pmatrix} 1 & 0 & 0 & 0 \\ 0 & \frac{1}{3} & 0 & 0 \\ 0 & 0 & -\frac{1}{3} & 0 \\ 0 & 0 & 0 & -1 \end{pmatrix}.
\end{aligned} \tag{A8}$$

The tensor operators can be defined similarly as follows

$$\begin{aligned}
\text{In } \Lambda_c \text{ and } \Sigma_c \text{ channels } &: \boldsymbol{\mathcal{O}}_{\text{ten}} = \frac{3(\boldsymbol{\sigma}_1 \cdot \mathrm{r})(\boldsymbol{\sigma}_2 \cdot \mathrm{r})}{\mathrm{r}^2} - \boldsymbol{\sigma}_1 \cdot \boldsymbol{\sigma}_2, \\
\text{In } \Lambda_c \to \Sigma_c^* \text{ and } \Sigma_c \to \Sigma_c^* \text{ channels } &: \boldsymbol{\mathcal{O}}_{\text{ten}} = \frac{3(\bar{\Sigma} \cdot \mathrm{r})(\boldsymbol{\sigma}_2 \cdot \mathrm{r})}{\mathrm{r}^2} - \bar{\Sigma} \cdot \boldsymbol{\sigma}_2, \\
\text{In } \Sigma_c^* \text{ diagonal channels } &: \boldsymbol{\mathcal{O}}_{\text{ten}} = \frac{3(\Sigma \cdot \mathrm{r})(\boldsymbol{\sigma}_2 \cdot \mathrm{r})}{\mathrm{r}^2} - \Sigma \cdot \boldsymbol{\sigma}_2,
\end{aligned} \tag{A9}$$

The spin-orbit operator $\boldsymbol{\mathcal{O}}_{LS}$ is defined as

$$\boldsymbol{\mathcal{O}}_{LS} = \boldsymbol{L} \cdot \boldsymbol{\sigma}_2. \tag{A10}$$

$\boldsymbol{L} \cdot \boldsymbol{\mathcal{O}}_1$ is not included in the potential for this calculation.

Appendix A.1. $I = \frac{1}{2}$, $J^\pi = 0^+$ *coupled system*

Tables A1-A3 give the matrix elements of $\boldsymbol{\mathcal{O}}_{spin}$, $\boldsymbol{\mathcal{O}}_{ten}$, and $\boldsymbol{\mathcal{O}}_{LS}$ for the channels in $I = 1/2$, $J^\pi = 0^+$. We label the relevant channels by i and j, and tabulate the ij component of the matrix elements $\langle \boldsymbol{\mathcal{O}} \rangle_{ij}$.

i \ j	$\Lambda_c N(^1S_0)$	$\Sigma_c N(^1S_0)$	$\Sigma_c^* N(^5D_0)$
$\Lambda_c N(^1S_0)$	-3	-3	0
$\Sigma_c N(^1S_0)$	-3	-3	0
$\Sigma_c^* N(^5D_0)$	0	0	1

Table A1 The matrix elements of the spin-spin operators $\langle \boldsymbol{\mathcal{O}}_{spin} \rangle_{ij}$ for the $I = \frac{1}{2}$, $J^\pi = 0^+$ coupled system.

i \ j	$\Lambda_c N(^1S_0)$	$\Sigma_c N(^1S_0)$	$\Sigma_c^* N(^5D_0)$
$\Lambda_c N(^1S_0)$	0	0	$-\sqrt{6}$
$\Sigma_c N(^1S_0)$	0	0	$-\sqrt{6}$
$\Sigma_c^* N(^5D_0)$	$-\sqrt{6}$	$-\sqrt{6}$	-2

Table A2 The matrix elements of the tensor operators $\langle \boldsymbol{\mathcal{O}}_{ten} \rangle_{ij}$ for the $I = \frac{1}{2}$, $J^\pi = 0^+$ coupled system.

i \ j	$\Lambda_c N(^1S_0)$	$\Sigma_c N(^1S_0)$	$\Sigma_c^* N(^5D_0)$
$\Lambda_c N(^1S_0)$	0	0	0
$\Sigma_c N(^1S_0)$	0	0	0
$\Sigma_c^* N(^5D_0)$	0	0	-3

Table A3 The matrix elements of the orbital-spin operators $\langle \boldsymbol{\mathcal{O}}_{LS} \rangle_{ij}$ for the $I = \frac{1}{2}$, $J^\pi = 0^+$ coupled system.

Appendix A.2. $I = \frac{1}{2}$, $J^\pi = 1^+$ *coupled system*

For $I = 1/2$, $J^\pi = 1^+$, the matrix elements are given in Tables A4-A6.

i \ j	$\Lambda_c N(^3S_1)$	$\Sigma_c N(^3S_1)$	$\Sigma_c^* N(^3S_1)$	$\Lambda_c N(^3D_1)$	$\Sigma_c N(^3D_1)$	$\Sigma_c^* N(^3D_1)$	$\Sigma_c^* N(^5D_1)$
$\Lambda_c N(^3S_1)$	1	1	$-\sqrt{\frac{8}{3}}$	0	0	0	0
$\Sigma_c N(^3S_1)$	1	1	$-\sqrt{\frac{8}{3}}$	0	0	0	0
$\Sigma_c^* N(^3S_1)$	$-\sqrt{\frac{8}{3}}$	$-\sqrt{\frac{8}{3}}$	$-\frac{5}{3}$	0	0	0	0
$\Lambda_c N(^3D_1)$	0	0	0	1	1	$-\sqrt{\frac{8}{3}}$	0
$\Sigma_c N(^3D_1)$	0	0	0	1	1	$-\sqrt{\frac{8}{3}}$	0
$\Sigma_c^* N(^3D_1)$	0	0	0	$-\sqrt{\frac{8}{3}}$	$-\sqrt{\frac{8}{3}}$	$-\frac{5}{3}$	0
$\Sigma_c^* N(^5D_1)$	0	0	0	0	0	0	1

Table A4 The matrix elements of the spin-spin operators $\langle \boldsymbol{\mathcal{O}}_{spin} \rangle_{ij}$ for the $I = \frac{1}{2}$, $J^\pi = 1^+$ coupled system.

i \ j	$\Lambda_c N(^3S_1)$	$\Sigma_c N(^3S_1)$	$\Sigma_c^* N(^3S_1)$	$\Lambda_c N(^3D_1)$	$\Sigma_c N(^3D_1)$	$\Sigma_c^* N(^3D_1)$	$\Sigma_c^* N(^5D_1)$
$\Lambda_c N(^3S_1)$	0	0	0	$\sqrt{8}$	$\sqrt{8}$	$\frac{1}{\sqrt{3}}$	$\sqrt{3}$
$\Sigma_c N(^3S_1)$	0	0	0	$\sqrt{8}$	$\sqrt{8}$	$\frac{1}{\sqrt{3}}$	$\sqrt{3}$
$\Sigma_c^* N(^3S_1)$	0	0	0	$\frac{1}{\sqrt{3}}$	$\frac{1}{\sqrt{3}}$	$-\frac{\sqrt{2}}{3}$	$-\sqrt{2}$
$\Lambda_c N(^3D_1)$	$\sqrt{8}$	$\sqrt{8}$	$\frac{1}{\sqrt{3}}$	-2	-2	$-\frac{1}{\sqrt{6}}$	$\sqrt{\frac{3}{2}}$
$\Sigma_c N(^3D_1)$	$\sqrt{8}$	$\sqrt{8}$	$\frac{1}{\sqrt{3}}$	-2	-2	$-\frac{1}{\sqrt{6}}$	$\sqrt{\frac{3}{2}}$
$\Sigma_c^* N(^3D_1)$	$\frac{1}{\sqrt{3}}$	$\frac{1}{\sqrt{3}}$	$-\frac{\sqrt{2}}{3}$	$-\frac{1}{\sqrt{6}}$	$-\frac{1}{\sqrt{6}}$	$\frac{1}{3}$	-1
$\Sigma_c^* N(^5D_1)$	$\sqrt{3}$	$\sqrt{3}$	$-\sqrt{2}$	$\sqrt{\frac{3}{2}}$	$\sqrt{\frac{3}{2}}$	-1	-1

Table A5 The matrix elements of the tensor operators $\langle \boldsymbol{\mathcal{O}}_{ten} \rangle_{ij}$ for the $I = \frac{1}{2}$, $J^\pi = 1^+$ coupled system.

i \ j	$\Lambda_c N(^3S_1)$	$\Sigma_c N(^3S_1)$	$\Sigma_c^* N(^3S_1)$	$\Lambda_c N(^3D_1)$	$\Sigma_c N(^3D_1)$	$\Sigma_c^* N(^3D_1)$	$\Sigma_c^* N(^5D_1)$
$\Lambda_c N(^3S_1)$	0	0	0	0	0	0	0
$\Sigma_c N(^3S_1)$	0	0	0	0	0	0	0
$\Sigma_c^* N(^3S_1)$	0	0	0	0	0	0	0
$\Lambda_c N(^3D_1)$	0	0	0	-3	-3	0	0
$\Sigma_c N(^3D_1)$	0	0	0	-3	-3	0	0
$\Sigma_c^* N(^3D_1)$	0	0	0	0	0	$\frac{3}{2}$	$-\frac{3}{2}$
$\Sigma_c^* N(^5D_1)$	0	0	0	0	0	$-\frac{3}{2}$	$-\frac{5}{2}$

Table A6 The matrix elements of the orbital-spin operators $\langle \boldsymbol{\mathcal{O}}_{LS} \rangle_{ij}$ for the $I = \frac{1}{2}$, $J^\pi = 1^+$ coupled system.

Appendix B. Definitions of the radial functions and coupling constants

Appendix B.1. The explicit forms of the radial functions

The Yukawa potential functions in Eq. (1) are defined as

$$
\begin{aligned}
Y(x) &= \frac{e^{-x}}{x}, \\
Z(x) &= (\frac{1}{x} + \frac{1}{x^2})Y(x), \\
H(x) &= (1 + \frac{3}{x} + \frac{3}{x^2})Y(x), \\
Y_1(m,\Lambda,r) &= Y(mr) - \left(\frac{\Lambda}{m}\right) Y(\Lambda r) - \frac{\Lambda^2 - m^2}{2m\Lambda} e^{-\Lambda r}, \\
Y_3(m,\Lambda,r) &= Y(mr) - \left(\frac{\Lambda}{m}\right) Y(\Lambda r) - \frac{(\Lambda^2 - m^2)\Lambda}{2m^3} e^{-\Lambda r}, \\
Z_3(m,\Lambda,r) &= Z(mr) - \left(\frac{\Lambda}{m}\right)^3 Z(\Lambda r) - \frac{(\Lambda^2 - m^2)\Lambda}{2m^3} Y(\Lambda r), \\
H_3(m,\Lambda,r) &= H(mr) - \left(\frac{\Lambda}{m}\right)^3 H(\Lambda r) - \frac{(\Lambda^2 - m^2)\Lambda}{2m^3} Y(\Lambda r) - \frac{(\Lambda^2 - m^2)\Lambda}{2m^3} e^{-\Lambda r}.
\end{aligned}
\tag{B1}
$$

In Eq. (B1), Λ is a cutoff parameter introduced in the monopole type form factor

$$
F(q) = \frac{\Lambda^2 - m^2}{\Lambda^2 - q^2}, \tag{B2}
$$

where m is the mass of the exchanged meson and q is the 4-dimensional momentum of the meson. We use the following values of the meson masses: $m_\pi = 137.27$[MeV], $m_\sigma = 600.0$[MeV].

Appendix B.2. The coupling constants for the meson-exchange potentials

The coupling constants are given in Tables B1 and B2,

C_π	$\Lambda_c N$	$\Sigma_c N$	$\Sigma_c^* N$
$\Lambda_c N$	0	$(-\frac{\sqrt{6}}{2} g_2 g_A)$	$-(\frac{\sqrt{6}}{2} g_4 g_A)$
$\Sigma_c N$		$(-g_1 g_A)$	$(-g_3 g_A)$
$\Sigma_c^* N$			$(g_5 g_A)$

Table B1 C_π for the $Y_c N$ systems

C_σ	$\Lambda_c N$	$\Sigma_c N$	$\Sigma_c^* N$
$\Lambda_c N$	$(2 l_B h_\sigma)$		
$\Sigma_c N$		$(-l_S h_\sigma)$	
$\Sigma_c^* N$			$(-l_S h_\sigma)$

Table B2 C_σ for the $Y_c N$ systems

with the following values [25–30]: and h_σ is a free parameter to be determined in sect.

$$
\begin{gathered}
g_2 = -0.598 \ , \ g_4 = 0.999 \ , \ g_1 = \tfrac{\sqrt{8}}{3} g_4 \ , \ g_3 = \sqrt{\tfrac{2}{3}} g_4 \ , \ g_5 = -\sqrt{2} g_4 \ , \\
g_A = 1.25 \ , \ l_B = -3.1 \ , \ l_S = -2 l_B,
\end{gathered}
$$

2.4 The explicit values of the coupling constants are given in Table B3 and B4 For the NN potential, we note that the function $Y_3(m,\Lambda,r)$ is used in place of $Y_1(m,\Lambda,r)$ in the π exchange potential and we adopt the coupling constants given in Tables B5 and B6.

C_π	$\Lambda_c N$	$\Sigma_c N$	$\Sigma_c^* N$
$\Lambda_c N$	0	0.92	-1.53
$\Sigma_c N$		-1.18	-1.02
$\Sigma_c^* N$			-1.77

Table B3 $Y_c N$ potential C_π values

C_σ	$\Lambda_c N$	$\Sigma_c N$	$\Sigma_c^* N$
$\Lambda_c N$	$(-6.2 h_\sigma)$		
$\Sigma_c N$		$(-6.2 h_\sigma)$	
$\Sigma_c^* N$			$(-6.2 h_\sigma)$

Table B4 $Y_c N$ potential C_σ values

C_π	$NN(I=0)$	$NN(I=1)$
$NN(I=0)$	$\frac{1}{2} g_A^2$	
$NN(I=1)$		$\frac{3}{2} g_A^2$

Table B5 C_π for the NN systems

C_σ	$NN(I=0)$	$NN(I=1)$
$NN(I=0)$	$-h_\sigma^2$	
$NN(I=1)$		$-h_\sigma^2$

Table B6 C_σ for the NN systems

Appendix C. Y_cN potentials

Here we show the shapes of the Y_cN potentials in the present study. The potentials for $J^\pi = 0^+$ are given in Figs. 3 - 8 in sect. 2.4.

Appendix C.1. Components of the Y_cn CTNN-a potential ($J^\pi = 0^+$)

The individual contributions of one-pion exchange, one σ exchange, and QCM repulsion are given in Figs. C1 - C3 for $J^\pi = 0^+$ CTNN-a potential. One sees that one σ exchange is strongly attractive, so that even with the QCM repulsion the total potential becomes attractive. The similar behavior is also observed for CTNN-b,c,d potentials.

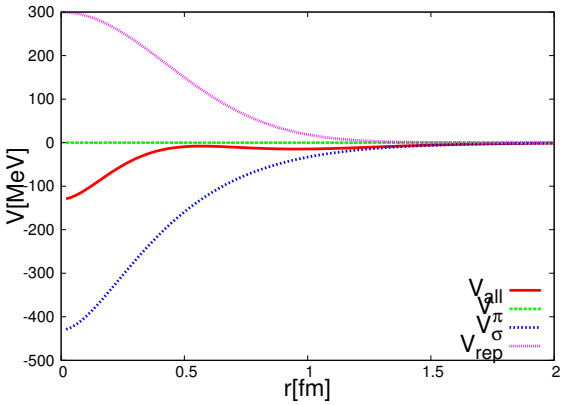

Fig. C1 Y_cN-CTNN potential for Λ_cN single channel

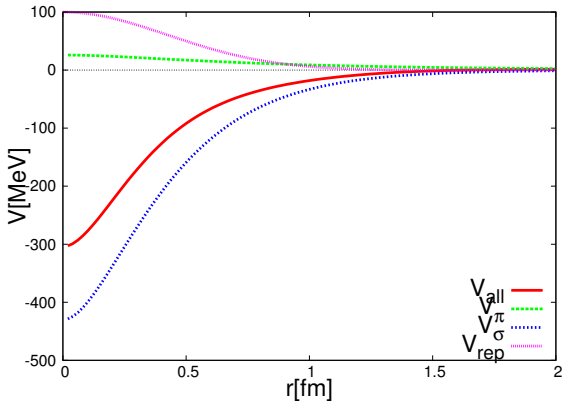

Fig. C2 Y_cN-CTNN potential for Σ_cN single channel

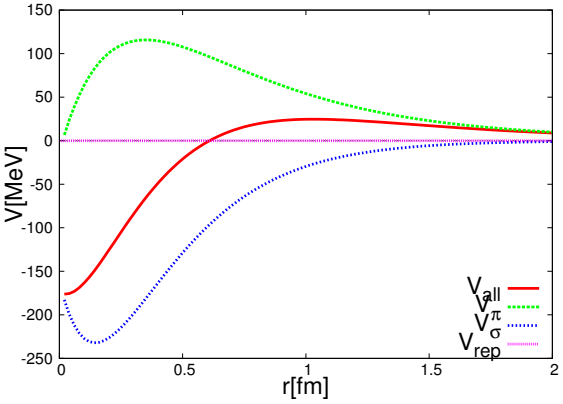

Fig. C3 Y_cN-CTNN potential for Σ_c^*N single channel

Appendix C.2. Y_cN potentials($J^\pi = 1^+$)

Figs. C4 - C29 show the $J^\pi = 1^+ Y_cN$ potentials. Four lines correspond to the four choices of the parameter sets, a $\sim$ d. The potential for the diagonal $\Lambda_cN(^3S_1)$ channel is not shown here as it coincides with that for $\Lambda_cN(^1S_0)$. The off-diagonal potential $\Lambda_cN(^3S_1 - ^3D_1)$ is zero.

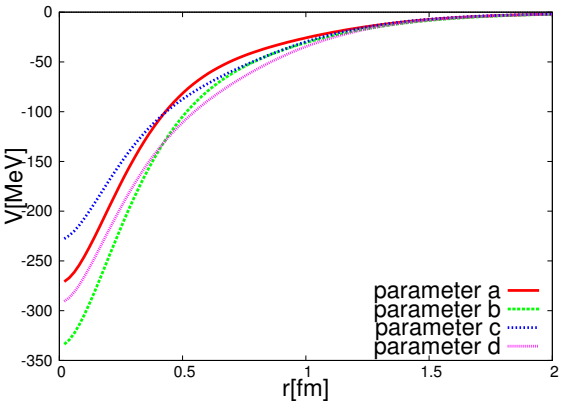

Fig. C4 $\Sigma_cN(^3S_1)$ diagonal potential.

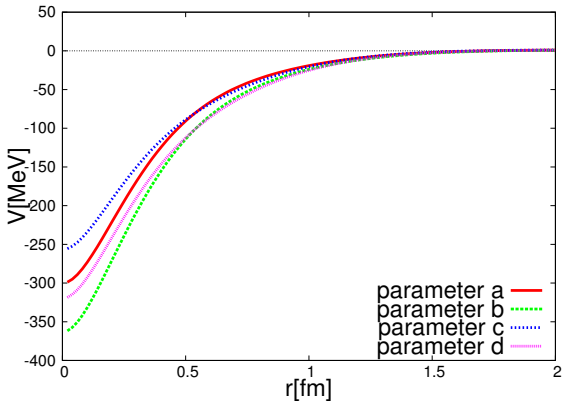

Fig. C5 $\Sigma_c^*N(^3S_1)$ diagonal potential.

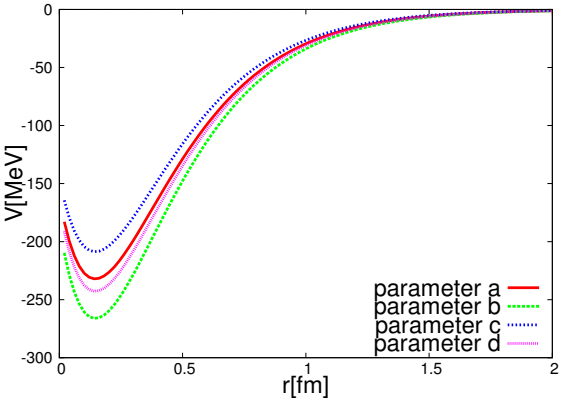

Fig. C6 $\Lambda_cN(^3D_1)$ diagonal potential.

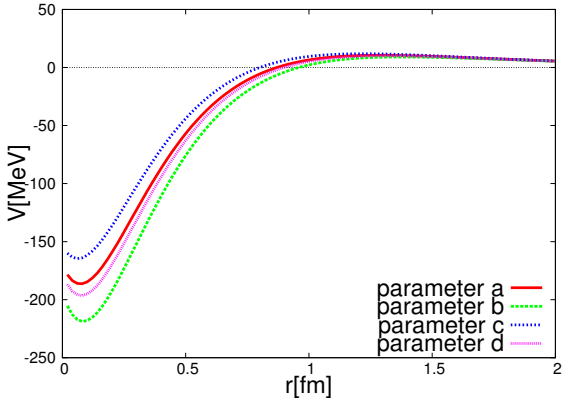

Fig. C7 $\Sigma_cN(^3D_1)$ diagonal potential.

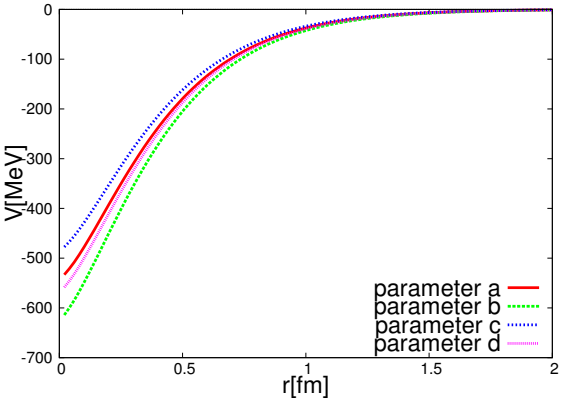

Fig. C8 $\Sigma_c^*N(^3D_1)$ diagonal potential.

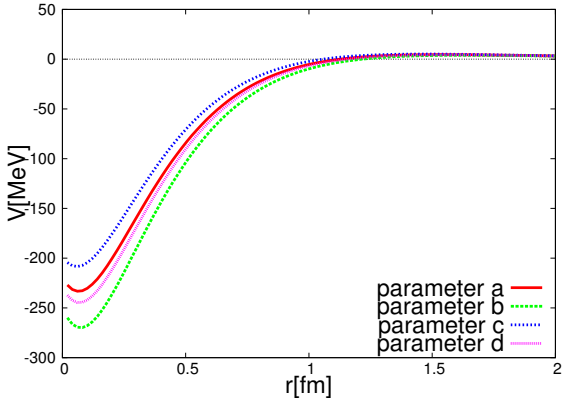

Fig. C9 $\Sigma_c^*N(^5D_1)$ diagonal potential.

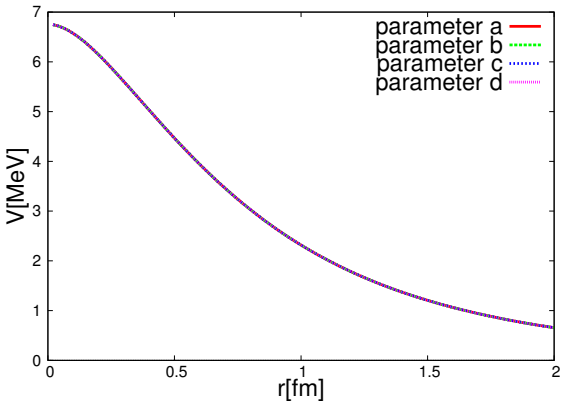

Fig. C10 $\Lambda_c N(^3S_1)$-$\Sigma_c N(^3S_1)$.

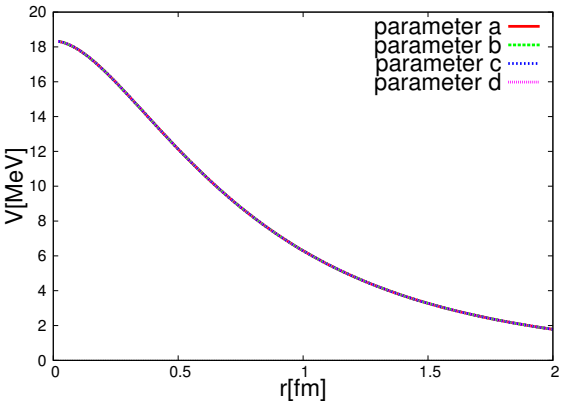

Fig. C11 $\Lambda_c N(^3S_1)$-$\Sigma_c^* N(^3S_1)$.

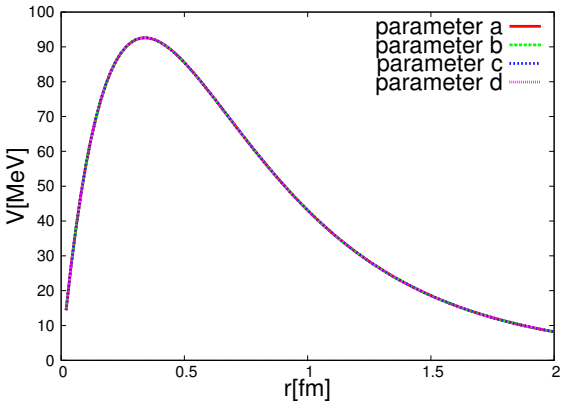

Fig. C12 $\Lambda_c N(^3S_1)$-$\Sigma_c N(^3D_1)$.

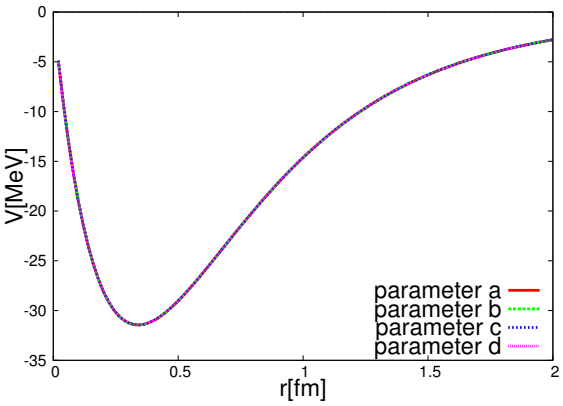

Fig. C13 $\Lambda_c N(^3S_1)$-$\Sigma_c^* N(^3D_1)$.

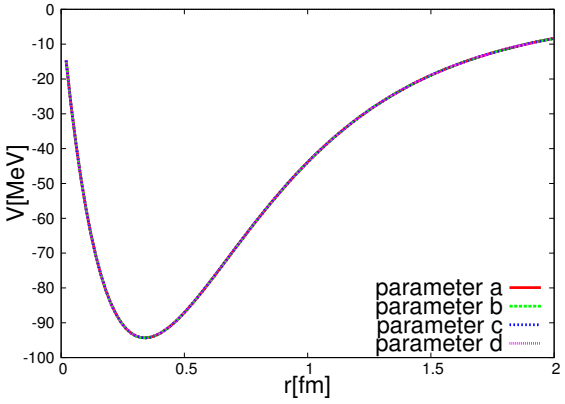

Fig. C14 $\Lambda_c N(^3S_1)$-$\Sigma_c^* N(^3D_1)$.

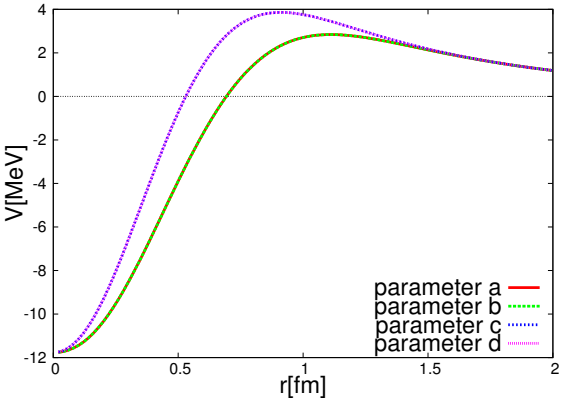

Fig. C15 $\Sigma_c N(^3S_1)$-$\Sigma_c^* N(^3S_1)$.

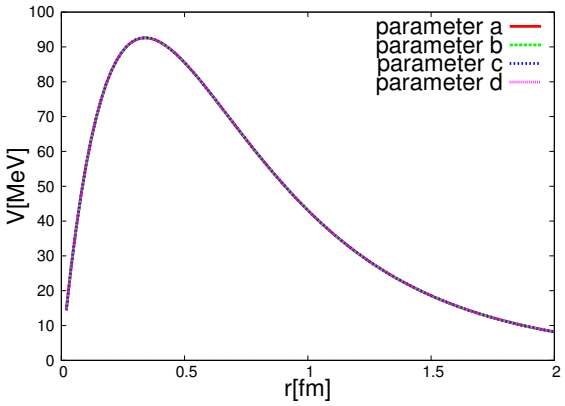

Fig. C16 $\Sigma_c N(^3S_1)$-$\Lambda_c N(^3D_1)$.

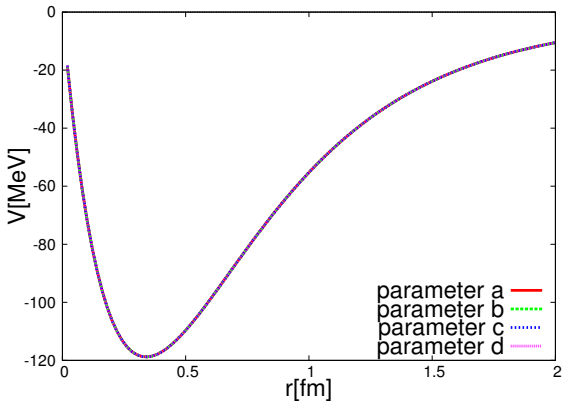

Fig. C17 $\Sigma_c N(^3S_1)$-$\Sigma_c N(^3D_1)$.

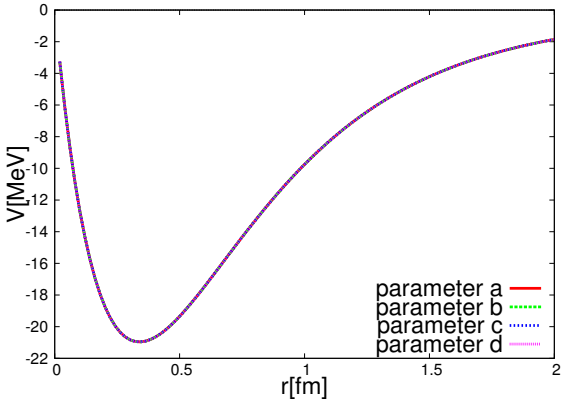

Fig. C18 $\Sigma_c N(^3S_1)$-$\Sigma_c^* N(^3D_1)$.

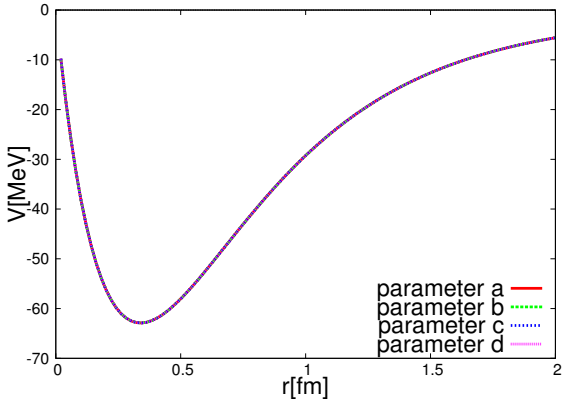

Fig. C19 $\Sigma_c N(^3S_1)$-$\Sigma_c^* N(^5D_1)$.

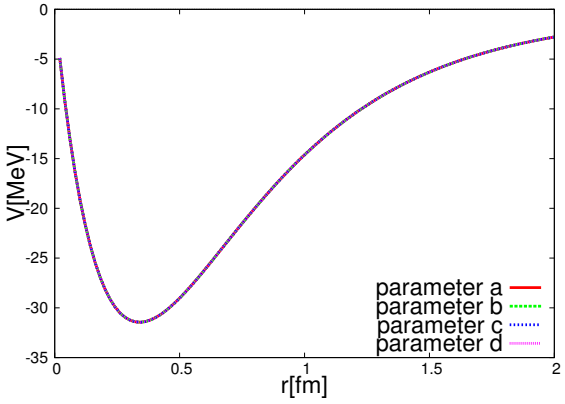

Fig. C20 $\Sigma c^* N(^3S_1)$-$\Lambda_c N(^3D_1)$.

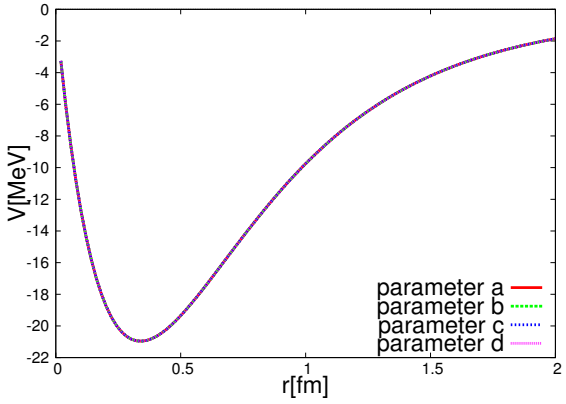

Fig. C21 $\Sigma c^* N(^3S_1)$-$\Sigma_c N(^3D_1)$.

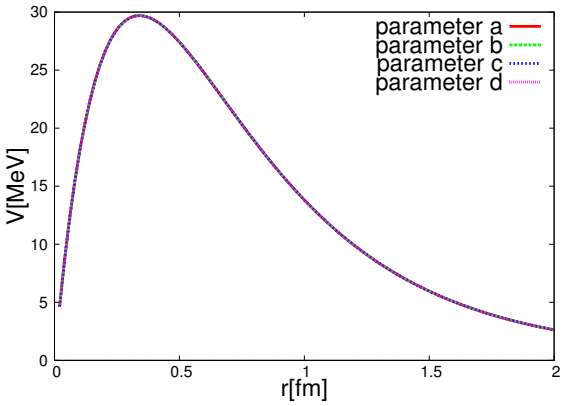

Fig. C22 $\Sigma c^* N(^3S_1)$-$\Sigma_c^* N(^3D_1)$.

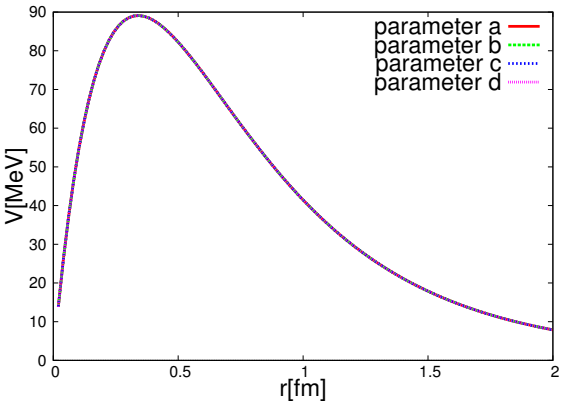

Fig. C23 $\Sigma c^* N(^3S_1)$-$\Sigma_c^* N(^5D_1)$.

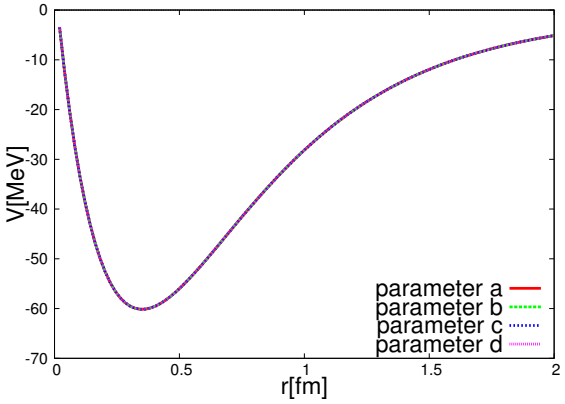

Fig. C24 $\Lambda c N(^3D_1)$-$\Sigma_c N(^3D_1)$.

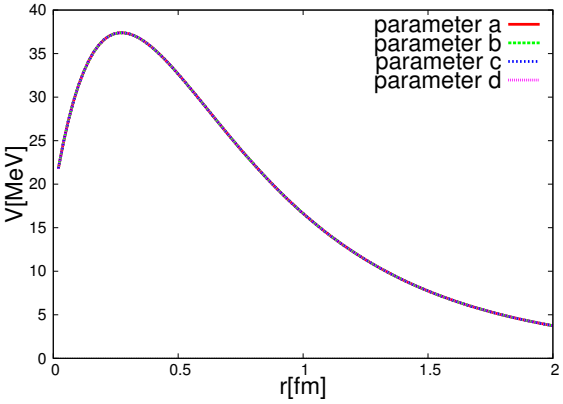

Fig. C25 $\Lambda c N(^3D_1)$-$\Sigma_c^* N(^3D_1)$.

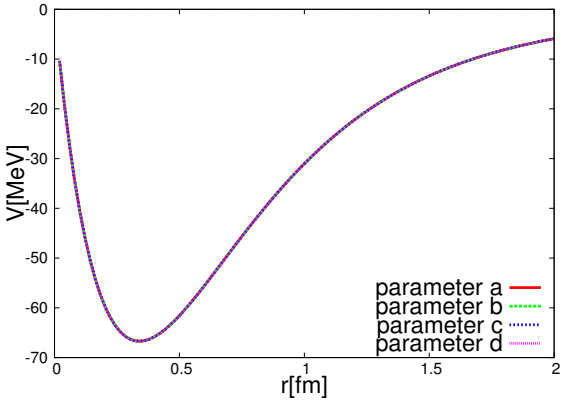

Fig. C26 $\Lambda c N(^3D_1)$-$\Sigma_c^* N(^5D_1)$.

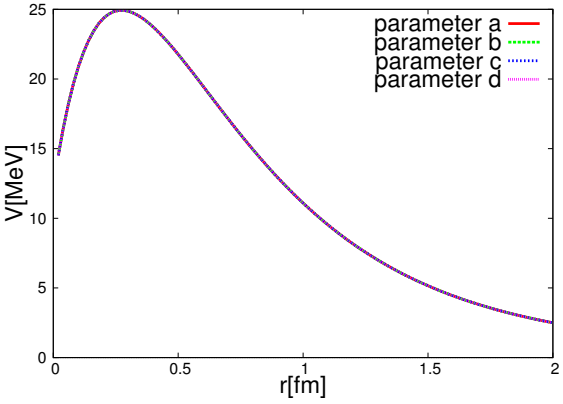

Fig. C27 $\Sigma c N(^3D_1)$-$\Sigma_c^* N(^3D_1)$.

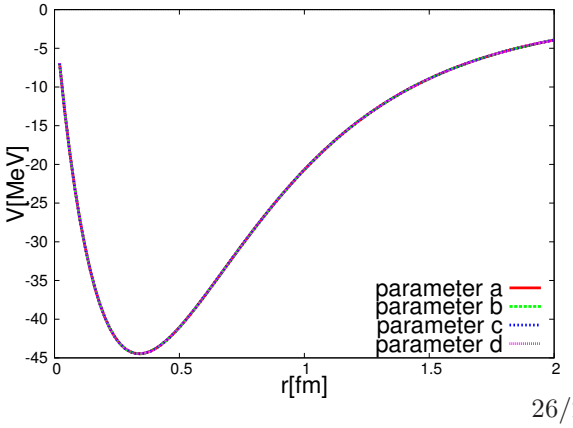

Fig. C28 $\Sigma c N(^3D_1)$-$\Sigma_c^* N(^5D_1)$.

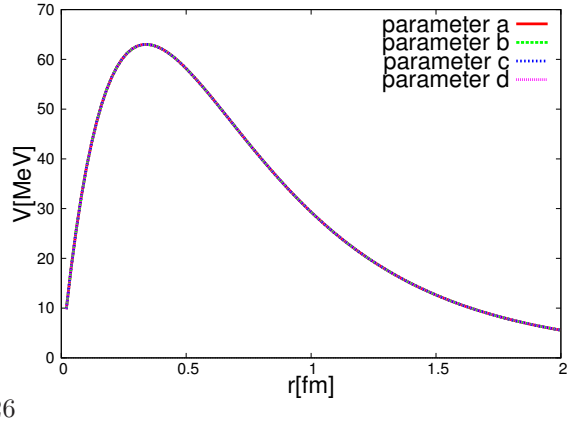

Fig. C29 $\Sigma c^* N(^3D_1)$-$\Sigma_c^* N(^5D_1)$.